BULLETIN OF THE POLISH ACADEMY OF SCIENCES
TECHNICAL SCIENCES
DOI: 10.24425/bpasts.2024.151957

Microstructural characteristics of a high-chromium cast iron hard-facing alloy

Teresa Fras[1], Benjamin Koenig[2], Paul P. Meyer[3], Ibra Diop[4]

[1] French-German Research Institute of Saint-Louis (ISL), Saint-Louis, France
[2] ENSTA Bretagne, Brest, France
[3] Department of Mechanical and Process Engineering, ETH Zürich, Switzerland
[4] Welding Alloys France, Holtzwihr, France

Abstract. Hard-facing alloys increase the service life of components exposed to abrasive, erosive, or metal-to-metal wear conditions. Hard-facing is a metalworking process in which layers of a harder material are arc-welded onto a base metal. In particular, high-chromium hard-face weld deposit layers form a strong metallurgical bond with the substrate steel plate, enhancing the resistance to abrasive loadings. Metallurgical and microstructural analysis is conducted to improve the performance of such bi-layered metal structures. The discussion of an HC-O hard-face alloy deposited on S235 steel substrate plates is hereby presented, focusing on the characterization of the coating's microstructure. The study establishes the relationship among the chemical composition, 'as-cladded' microstructure, and hardness properties of the investigated high chromium Fe–27 wt.% Cr–5 wt.% C hard-facing alloy.

Key words: arc welding, FCAW, hard-facing alloys, HC-O, high-chromium cast iron, EBSD, micro-hardness

1. INTRODUCTION

Hard-facing has been adopted as an effective manufacturing technology to improve the mechanical and tribological properties of components subjected to abrasive wear. Hard-facing is a metalworking process in which a harder or tougher material is cladded onto a base metal by a specialized electrode in arc-welding. The microstructure of the cladding layer is improved by the presence of carbides dispersed in the austenite matrix. The process of hard-facing concerns industrial components such as crushers, rolls, extruder screws, mining and earthmoving equipment, blast furnace bells, wear plates, etc. [1]. Strong carbide formers (such as chromium, titanium, vanadium, or tungsten) are used as the main alloying elements in the surfacing materials [2-3]. Tungsten or vanadium-rich alloys offer a good combination of high hardness and high toughness, but they are more expensive than chromium-rich alloys. Iron-chromium-carbon (Fe-Cr-C) alloys are widely used in hard-facings since they possess high hardness, high tribological performance, and a good cost-benefit ratio [4-6].

High-chromium cast irons (with 10–30 weight percent Cr) make up almost all hypoeutectic alloys utilized for abrasion resistance [7]. Alloys with 12 wt.% Cr are the least expensive, whereas the most common are 18–22 wt.% Cr irons because of their good abrasion resistance. They are often used as rollers and tables in coal pulverizing or as liners in dry ball mills. The alloys with 2.0–2.7 wt.% C and 27–30 wt.% Cr were developed specifically for wet wear applications that require both corrosion and abrasion resistance. For high-temperature applications, such as furnace and burner parts, irons with a weight percentage of 30–35 wt.% Cr are utilized to prevent oxidation and corrosion. The welding process conditions (i.e., the temperature of weld pool melt overheating and cooling conditions) and the deposited metal composition determine the nature of formed carbides and their arrangement in the structure. The resulting carbide arrangement and shapes of their precipitates significantly influence the resulting material properties.

Studies on hard-facing alloys are a thriving part of tribological and surfacing studies. Various processes used for the laying down of hard-facing materials on metallic surfaces are described by Henderson et al. [8]. In addition, a classification of hard-facing alloy types based on particles of the primary carbide phase dispersed in an iron-rich matrix and their properties is analyzed. Ryabtsev et al. [4] described the wear resistance in cladded layers deposited by a flux-cored wire strengthened by titanium and chromium carbides. The results of an X-ray diffraction analysis and SEM and LEM microscopic observations of high-Cr white cast iron are presented by Ban et al. [9], who confirmed that the microstructures of the welded layers are characterized by fine and hard chromium carbides densely dispersed in the iron matrix. It is implied that the wear resistance is enhanced with an increase in the coverage rate of carbides to the matrix, along with a more dense dispersion of the finer and harder carbides, resulting in mechanical support, which decreases the effects of abrasion. Sa de Sousa et al. [10] assessed the abrasion resistance of Fe-C-Cr alloy coatings deposited by the Flux-Cored Arc Welding (FCAW) process. They observed that the coatings possess a resistant metallurgical bond and a

good surface quality concerning the uniformity and absence of defects. The investigated microstructure was composed of carbides dispersed in a Fe eutectic matrix, whose characteristics varied according to the dilution level and deposition parameters. It was confirmed that the coatings with a higher volume fraction and a lower mean free path between the carbides showed a lower wear rate average and less severe aspects of worn surfaces.

This study uses chromium-based wires to obtain a strengthening phase in the hard-face alloying processes. The hard-facing HC-O welded on the base-steel substrate S235 is the cladded coating hereby investigated. According to the producer of the hard-facing alloy, the content of Cr is a minimum of 27 wt.%. The study's objective is to provide an insight into the microstructure of an HC-O alloy produced by a self-shielded Flux-Cored Arc Welding (FCAW) process. The microstructural analysis is based on a Light-Optical and scanning electron Microscopic (LOM and SEM) examination complemented by an Electron Backscatter Diffraction (EBSD) investigation, due to which a local crystal structure and the grain orientation were analyzed. Further, the micro-hardness of the tested coating was verified. The properties of the HC-O hard-face deposit were investigated in the 'as-cladded' conditions.

2. CHEMICAL COMPOSITION OF THE BI-LAYERED PLATE

In the investigated bi-layered plate, 6 mm-thick steel plates made of structural steel S235 were used as the substrate. The S235 steel is a readily weldable low-carbon manganese steel with a regulated chemical composition. Therefore, its mechanical and material properties remain the same independently of the manufacturer [11].

TABLE 1. Chemical composition of the substrate steel S235 and the filler metal HC-O, [11-12]

	Chemical composition, % by weight					
	Cr	**Mn**	**C**	**P**	**Si**	**Fe**
Substrate steel S235		1.6	0.22	0.05	0.05	Rest
Self-shielded flux-cored wire hard-face HC-O	>27	1.5	5.0		1.5	Rest

The hard-face HC-O alloy used here is sold as tubular wire for self-shielded metal arc hard-facing [12]. The resulting structure is a high-chromium cast iron deposit containing a high proportion of hard primary chromium carbides in a tough ferrous matrix. Such a hard-face layer suits components subjected to extremely severe abrasive wear and moderate impact. The chemical composition of the weld deposit of the filler metals is presented in Table 1, along with the data concerning the S235 steel [11-12].

TABLE 2. Hard-facing process parameters.

Current intensity [A]	**Arc voltage, [V]**	**Welding speed, [m/min]**	**Wire feeding speed [m/min]**	**Wire extension, [mm]**	**Bead offset [mm]**
300+-50	24+-0.5	1.7	5.1	25	3.0

An approximate 3 mm layer of the hard-face HC-O layer was deposited on the top of the steel plates by automatic self-shielded Flux-Cored Arc Welding (FCAW). The FCAW welding process does not require an additional shielding gas. Since it is a continuous semi-automatic process, it may be commonly used as a hard-facing technique suitable for all sizes and welding positions. Bead-on-plate was made with an electric power supply using an auto-mechanized system provided by an H-Frame welding machine, in which the welding torch was moved back and forth at a constant speed above the alloy filler. The hard-facing fillers were deposited on the steel base metal by the self-shielded FCAW process using the welding parameters shown in Table 2.

Figure 1 presents a detailed view of the welded deposit. The deposit, which has an approximate size of 150×150 mm, consists of 30–40 deposited beads with an approximate width of 4–4.5 mm. In the fragment of the cross-section shown in Fig. 1(b), the total height of the bi-layered plates measures 8.1–8.3 mm. The width of the cladded layer, a key characteristic of the deposit, varies between 1.8 and 2.7 mm, demonstrating the variability of the welding process.

(a)

(b)

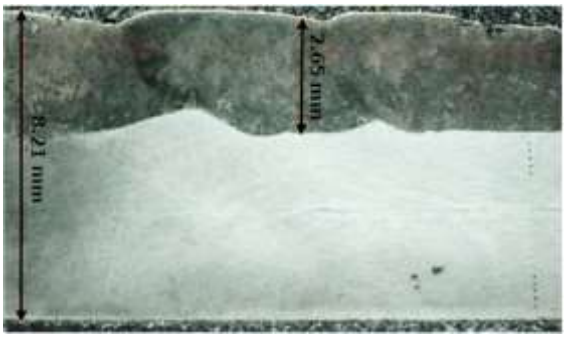

Fig.1. (a) HC-O hard-face plate produced by an automatized arc-welding process performed by an H-Frame welding machine, (b) fragment of the cross-section.

The conditions of cooling, solidification, precipitation, and phase change in Fe–Cr–C alloys depend on the FCAW process's deposition parameters. The filler and a thin surface layer of the substrate steel are melted and then rapidly solidified to form a dense cladding layer that bonds the two structures. The surfacing technology, as well as the microstructure and the composition of the powder (that makes up the filler material), affect the resulting structure of the crystallized hard-faced metal. Therefore, a microstructural analysis provides an insight that may explain the phenomenological behaviour of the manufactured plates.

3. PHASE DIAGRAM OF THE CLADDED HARD-FACE HC-O LAYER

An X-Ray Diffraction (XRD) measurements on the HC-O hard-faced deposit were conducted to analyse the chemical composition. Cooling during the welding process, as well as usage of a wire overloaded with chromium, resulted in a through-thickness constant chromium/carbon ratio and a similar carbide content after a dilution, as presented in Fig. 2. Following examples given in [5, 10, 13-15], the figure shows the liquidus projection of the iron corner of the Fe–Cr–C ternary system updated for the investigated structure. The x-sign marks the chemical composition indicated by the wire producer [12]. The calculation of the element's content is based on the analysis of the spots indicated as (1)–(4) in Fig. 3. This chemical composition analysis indicates the occurrence of M_7C_3 carbides in the structure of the cladded hard-face layer.

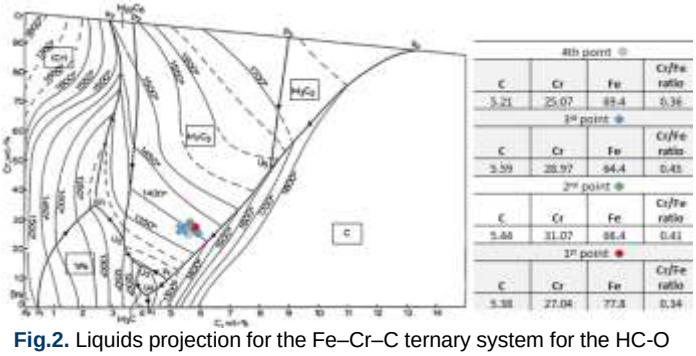

Fig.2. Liquids projection for the Fe–Cr–C ternary system for the HC-O deposit

High-chromium-cast iron solidifies into a ferritic matrix with chromium carbides. The carbide types known to be present in the high-chromium cast irons are M_7C_3, M_3C, $M_{23}C_6$, and M_6C carbides [7, 16-17]. Wear resistance and mechanical properties of high-chromium cast irons depend on the eutectic and precipitated carbides and the nature of the matrix supporting them. The type and morphology of the eutectic carbides in high-chromium-cast iron depend upon both chemical composition and solidification rate [7, 16-17]. The eutectic carbide structure in high-Cr irons is strongly influenced by chromium since chromium has a stronger tendency to form carbides than iron. In lower chromium irons with less than 12 wt.% Cr, the eutectic carbide is M_3C with an orthorhombic crystal structure and a hardness of around 1000 HV. Below about six wt.% Cr, this carbide is in a continuous form, which limits the toughness. When the amount of Cr is about 8–10 wt.% Cr, the eutectic carbides are less continuous and can be duplex, consisting of an inner core of M_7C_3 and an outer shell of M_3C formed during solid-state cooling. Increasing the chromium and carbon contents in white iron changes the carbide type from the continuous M_3C to the lamellar M_7C_3, increasing toughness. Above 12 wt.% Cr, the carbide changes to the M_7C_3 type. The M_7C_3 carbide has a pseudo-hexagonal structure containing 56 iron and 24 carbon atoms. M_7C_3 carbides consist of rod-like hexagonal pencil-shaped crystals, solidifying as a colony structure to form blade-like structures. These M_7C_3 carbides become finer with increasing chromium content and an increasing eutectic solidification rate. They have a hardness of around 1400–1600 HV.

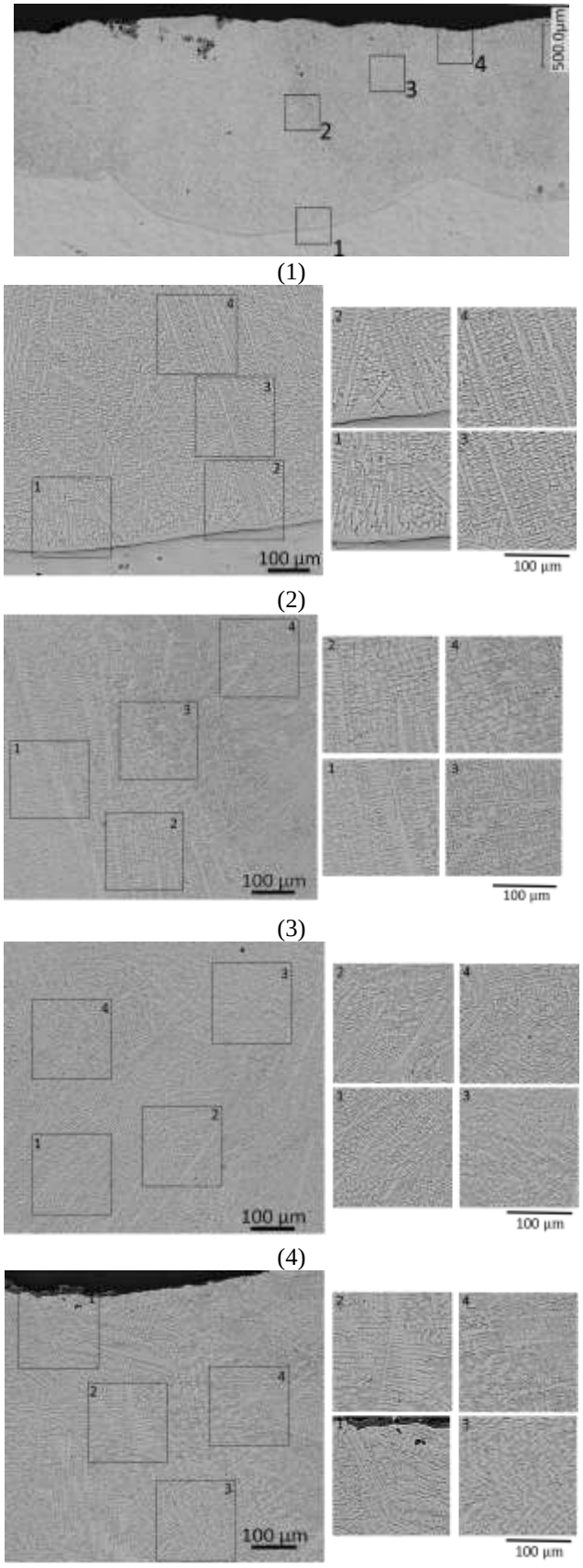

Fig.3. LOM micro-graphs showing the HC-O welded structure's microstructure

During conventional destabilization or annealing treatments, the eutectic M_7C_3 carbides in 10–25 wt.% Cr irons do not undergo any structural change. However, in the 30 wt.% Cr irons, a transition from M_7C_3 to $M_{23}C_6$ has been observed in the eutectic carbides [7], which results in duplex eutectic carbide structures consisting of cores of M_7C_3 surrounded by shells of $M_{23}C_6$. The extent of the transformation depends on destabilization temperatures and time. This transformation has only been observed within the very high chromium content irons (where the $M_{23}C_6$ carbides remain stable [16]). It is supposed that the $M_{23}C_6$ carbides nucleate at the original interface between the matrix and the eutectic M_7C_3 carbides. As the $M_{23}C_6$ phase expands, it gains metal atoms from the matrix and devours the M_7C_3. TEM investigation would be required to fully unveil details of the structure, particularly to distinguish between the M_7C_3 and $M_{23}C_6$ carbides; allowing also a better understating of transition between the two carbide types [7, 17].

4. MICROSTRUCTURE OF THE WELDED DEPOSIT

The LOM and SEM micrographs of the HC-O welded deposit are given in Figs. 3–4 for different zones along the longitudinal cross-section. The microstructure has been analyzed using light electron microscopy by Keyence VHX Digital Microscope (LOM) and a FEI Scios dual-beam Scanning Electron Microscope (SEM). The Electron Back Backscatter Diffraction (EBSD) technique was applied to shed light on the structural characteristics, generating insightful images of the polycrystalline microstructure. The microstructure of the cladding layer in two mutually orthogonal directions to the substrate surface is shown in Figs. 5–6. Before the EBSD analysis, the extracted samples were subjected to mechanical grinding with silicon carbide paper, followed by a final polishing step using a 60 nm alumina colloid. Subsequently, the EBSD acquisitions utilizing a scanning electron microscope operating at an accelerating voltage of 20 kV were undertaken.

In Fig. 3(a), a joint typical for welded structures may be observed (e.g. [18-19]). The depicted bead is 3.6 mm long. The images collected in Fig. 3 also show that the cladded HC-O layer has a fine structure, and no cracks or precipices are present, which confirms that both the cladded layer structure and the bond are of a high quality. The middle zone of the welded HC-O is shown in Figs. 3(c-d). The cladding layer appeared very stable with a low dilution, due to which well-developed columnar dendrites occurred. A few close-ups from different zones confirm this observation of the structural morphology, Figs. 4(a-c).

After the welding process, cooling is initiated; the first phase to become solid is the austenite dendrites, which are visible in the images. The grain growth rate and temperature gradient in the liquid and alloy chemical composition are among the variables that have the greatest influence on solidification morphology. Depending on how these conditions are exerted, the solid-liquid interface might develop through the growth of planar, cellular or dendritic grains. As the solidification continues, the primary austenite dendrites reject C and Cr from the remaining liquid, which these elements enrich until the eutectic composition (e.g. [20-21]). Further, the serrated microstructure features are observed in Fig. 4(c), which can be identified as primary carbides M_7C_3 (here, the (Fe, Cr)7C3 carbides) grown within the austenite matrix. Other researchers also report similar observations, e.g., [5-7, 20-24]. The formation of proto-grains at the interface between the bead and the substrate indicates that the maturation of the dendrites into grains has occurred, as shown in Fig. 3(b), as well as in Figs. 4(b, d). The interface microstructure between the steel substrate and the cladded layer reveals a thin layer (20 µm to 40 µm) of epitaxial solidification with a planar front growth. The remaining liquid decomposes into a mixture of austenite and M_7C_3 eutectic carbides [23]. The M_7C_3 primary carbides are the first phase to be formed in cooling below the liquidus temperature. High cooling rates can reduce the size of the carbides or even prevent their formation [10]. Despite the fast nucleation of these carbides, their growth kinematics is slow. They need a certain period before the completion of the solidification, which allows for their full development.

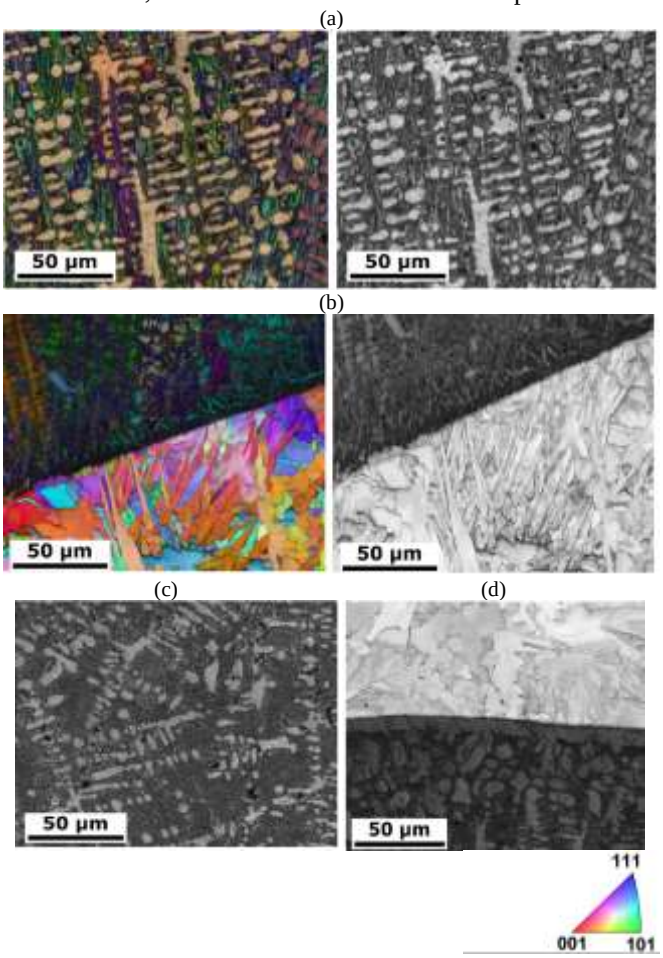

Fig.4. SEM images of some microstructural details. Middle of the cladded layer: (a) and (c). Interface between the steel substrate and the deposit: (b) and (d)

The M_7C_3 phase in the analyzed structure corresponds to chromium carbide $(Fe, Cr)_7C_3$-type. The $(Fe, Cr)_7C_3$ carbides have good wear resistance properties because of extremely high hardness, as reported by [5-7, 20-23]. Because of a high $(Fe, Cr)_7C_3$ content, Fe–Cr–C white cast irons are used as hard-facing alloys. In abrasion-resistant coatings, M_7C_3 carbides increase surface hardness, hindering the penetration

of abrasive particles. These phases provide a barrier effect to the nucleation and propagation of wear micro mechanisms. The authors of [25-27] demonstrated that most of the carbide rods are hollow, of hexagonal cross-section, and grow preferentially along the [0001] axis (perpendicular to the hexagonal basal plane). The diameter of the carbide rods is typically between 1 and 4 µm. In contrast, the hollow core, filled with matrix material of the same composition as that adjacent to the carbides, has a diameter between 0.2 and 0.6 µm. The carbide's eutectic regions grow in colonies, like the rosettes of eutectic cells shown in the magnification in Fig. 4(c).

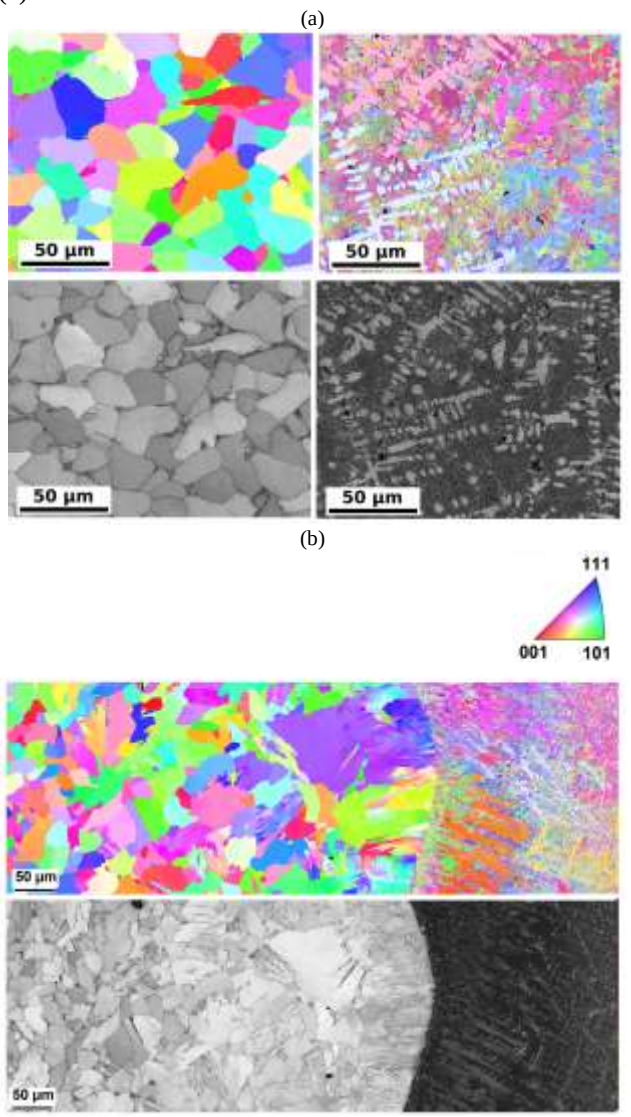

Fig.5. EBSD images parallel to the building direction of the HC-O layer: (a) inside the layer, (b) between the steel substrate and the cladded deposit

The objective of the EBSD analysis was to capture a representative scan area, utilizing a spatial step size of 0.2 µm to ensure a high-resolution examination of the microstructure. The Inverse Pole Figures (IPF) offer insights into the crystallographic orientation within these materials. Far from the interface, the grains within the base material exhibited a homogeneous morphology, characterized by an average size of approximately 20 µm and an absence of preferred orientation both in-plane and transverse to the building direction, Fig. 5(a). However, in proximity to the boundary between the base material and the cladding layer, a significant transformation was evident. At this location, the grains within the base material displayed elongation perpendicular to the boundary, and their width was reduced to only a few micrometers, Fig. 5(b). This microstructural alteration was particularly pronounced when assessed transverse to the building direction. The zone featuring this distinctive grain texture extended approximately 100 µm into the base layers. Beyond this region, the grains within the base material became markedly larger and exhibited reduced homogeneity in shape compared to the bulk of the base material. Notably, at approximately 400 µm from the boundary, the grains within the base material reverted to a morphology indistinguishable from the bulk material, suggesting a gradual transition and re-establishment of the material's inherent characteristics.

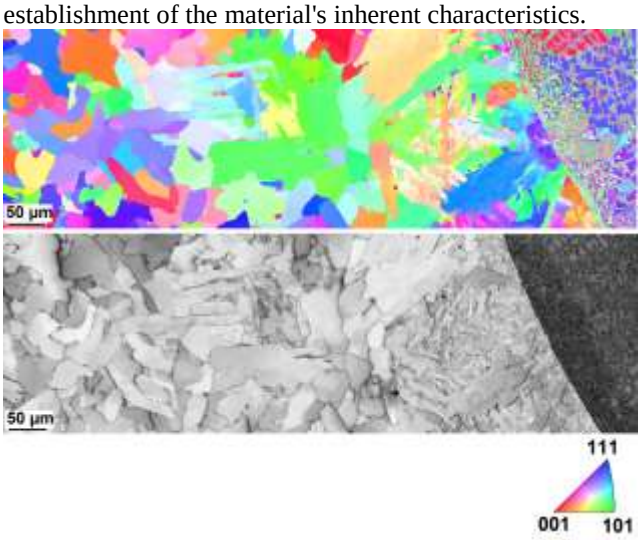

Fig.6. EBSD images orthogonal to the building direction of the transition between the steel substrate and the cladded deposit

At approximately 20 µm from the boundary, the dendrites exhibit a much finer structure compared to those found farther from the boundary, as shown in Fig. 5-6. This finer-structured layer extends over a length of about 20 µm before a marked change occurs. The boundary proximity appears to influence the dendritic growth, as the dendrites exhibit a pronounced preferential growth direction perpendicular to the boundary. However, this preferential growth direction gradually fades as one moves approximately 200 µm away from the boundary. At this distance, the dendrites self-organize into patches comprising numerous dendrites, all aligned in the same growth direction. Further along the building direction, the dendrites extend to lengths exceeding 80 µm, while perpendicular to this direction, their length is significantly shorter, approximately 50 µm, forming a distinct spatial distribution near the material boundaries.

A sharp transition, characterized by an absence of intermixing, is observed between these two material layers. The introduction of heat during cladding substantially influenced the grain structure of the base material near the boundary with the cladding layer. At this interface, we have documented the reformation of grains and observed perpendicular grain growth, illustrating the base material's

remarkable sensitivity to cladding's thermal effects. Notably, the orientation of dendrites displayed a distinct pattern along the temperature gradient, with a pronounced alignment close to the boundary. As one moves further from the boundary, this preferential orientation becomes less pronounced, and dendrites exhibit larger growth.

These observations can be attributed to the efficient conduction of heat away from the cladding layer by the base material, resulting in steeper temperature gradients perpendicular to the boundary. To produce coatings with high mechanical properties, an adequate adhesion between the substrate and reinforcing phase is necessary [28]. Although the bond's strength was not confirmed (for instance, by a scratch test), it would be an important experimental output explaining the interface performance in response to different loadings.

5. HARDNESS MEASUREMENTS

The Vickers micro-hardness (HV) measurements were conducted to elucidate the influence of microstructural alterations induced during the cladding process on the mechanical properties of the structure. The same surface preparation as for the EBSD analysis was used to conduct unaltered hardness measurements on flat surfaces. To ensure the reliability of the findings, several measurements were performed across multiple locations and load settings during the indentation process, which are presented in Fig. 7(a). These indentations are performed and measured sequentially. In addition, the measurements are validated with individual intentions several millimeters away to exclude any influence by other indentation. Employing a Qness Q10M, HV measurements along lines perpendicular to the boundary at fixed intervals were conducted, examining the localized variations in material hardness, shown in Fig. 7(b). Three zones may describe the hardness graph along the measured width: the steel base substrate (B), the transition zone (T), and finally, the Cladding Layer (CL). The red measurements use a mass of 0.05 kg and are placed in the base substrate and transition zone. The blue measurements transition the entire sample and switch from a mass of 1 kg in the base substrate to 5 kg in the cladding layer to keep insertion depth and diameter constant. The orange measurements focus on the transition from base substrate to cladding layer and use a mass of 1 kg. The green measurements serve as validation across the sample using a mass of 2 kg. The purple measurements are conducted orthogonal to the building direction and use a mass of 1 kg. Despite the pronounced changes in grain structure, the measurements indicated that the micro-hardness of the material remains unaffected. Remarkably consistent hardness measurements for the base material, averaging around 110 HV1, across various measurement points are observed. Notably, in proximity to the boundary, where the indentation size was approximately 100 µm, and the measurement spacing was roughly 300 µm, no discernible increase in base material hardness was observed. Within the cladding layer, a sharp increase in hardness was detected. Unavailable, for now, measurements with smaller intenders in this narrow zone would allow us to observe a detailed character of hardness changes in the transition zone. The average hardness within the cladding layer was measured as approximately close to 775 HV1. A noticeable distinction may be remarked between the measurements parallel (green, orange, blue, and red dots of various size indentions) and the average level of hardness of approximately 700 HV1 and the measurements perpendicular to the building direction (marked by the violet dots) of values approximately close to 850 HV1. The high hardness of the HC-O deposit results from its dense structure, which was obtained due to a high energy density laser treatment and the presence of carbide phases.

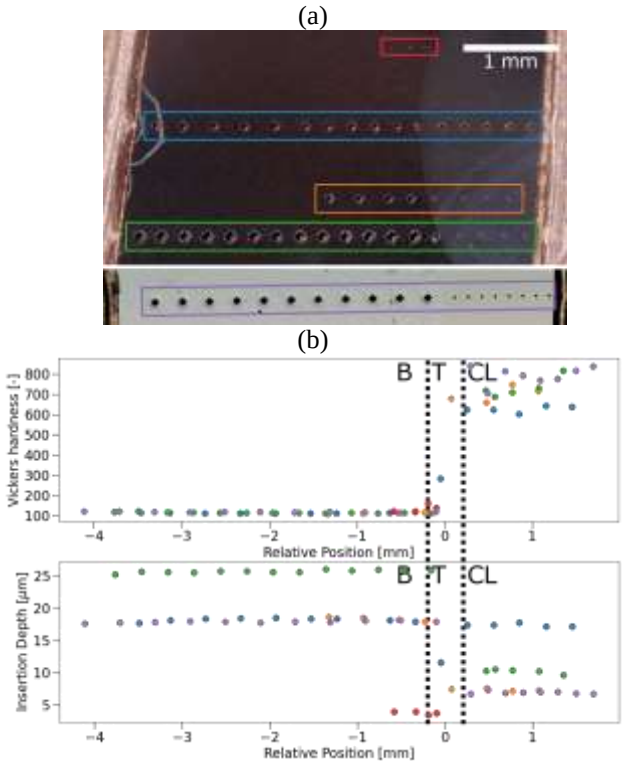

Fig.7. Hardness measurements along the thickness of the two-layered structure: (a) schema of intenders' positions, (b) through-thickness hardness measurements and corresponding insertion depth

6. CONCLUSIONS

The primary goal of the hard-facing processes is to increase the lifespan of industrial components by covering surfaces that are prone to corrosion, wear, or abrasion with more resistant alloys. The objective of manufacturing the hereby analyzed double-layered plates was to enhance the protective properties of the conventional construction steels [29]. The presented results are a part of an ongoing project in which further findings regarding the material and mechanical properties, as well as anti-perforation performance, should be available in the future.

In this study, an analysis of the microstructure of the bi-layered metal plates manufactured by self-shielded flux-cored arc welding was conducted. The base substrate is the steel S235 on the top, on which hard-face HC-O was cladded. About 3 mm of the hard-face HC-O layer was deposited on the top of the steel plates by automatic self-shielded flux-cored arc welding. Applying a cooling system during welding and using a wire overloaded with chromium resulted in a constant through-thickness chromium / carbon ratio and a similar carbide content after dilution. The cladded HC-O layer

has a fine structure, and no cracks or precipices are present, confirming that the cladded layer structure and the bond are high quality.

The SEM and LOM images showed that in the 'as-deposited' state, the hard-face alloy is characterized by the structure with the morphology of the dendrites and the eutectic carbides. On LOM images, a well-developed columnar dendrite structure through the thickness of the whole layer is seen. Simultaneously, the eutectic M_7C_3 carbides may exhibit a fine rod-like morphology in SEM images. Further, the consistent hardness measurements for the base material, averaging around 110 HV1, across various measurement points were obtained. The average hardness within the cladded layer was measured as approximately close to 775 HV1. No investigation on the abrasion or corrosion properties of the base material, nor on the final structure, was yet performed.

The obtained results provide an insight into the complex microstructure of the HC-O-deposited hard-face layer and its evolution with respect to distance from the boundary, highlighting the dynamic nature of dendritic formation in the structure.

ACKNOWLEDGEMENTS

The help of Mr. Quentin Marchal is hereby acknowledged.

AUTHOR CONTRIBUTIONS

T.F. conceived, formulated and supervised the project. B.K. and I.D. performed the hard-facing process and analyzed the chemical composition. B.K. and P.M. executed the LOM measurements. P.M. executed and analyzed the EBSD and hardness measurements. T.F., B.J., P.M. and I.D. discussed the results and co-wrote the manuscript.

REFERENCES

[1] B. Gerard. Fundamentals of Hardfacing by Arc Welding. Welding Alloys: Florence, KY, USA, 2016; pp. 1–47.

[2] D. Tandon, H. Li, Z. Pan, D. Yu, and W. Pang, "A Review on Hardfacing, Process Variables, Challenges, and Future Works," Metals vol. 13. No. 9, pp. 1512, 2023. https://doi.org/10.3390/met13091512.

[3] A. Krajewski, A. Włosiński, W. Chmielewski, P. Kołodziejczak, "Ultrasonic-vibration assisted arc-welding of aluminum alloys," Bull. Polish Acad. Sci. Tech. Sci., vol. 68, no.4, pp. 841–852, 2012. https://doi.org/10.2478/v10175-012-0098-2.

[4] I.A. Ryabtsev, A. I. Panfilov, A. Babinets, I. I. Ryabtsev, G. N. Gordan and I. L. Babijchuk, "Structure and abrasive wear resistance of deposited metal hardened with carbides of different types," The Paton Welding J., vol. 5, no. 6, pp. 78–82, 2015.

[5] H. Sabet, S. Khierandish, S. Mirdamadi, M. Goodarzi, "The microstructure and abrasive wear resistance of Fe-Cr-C hardfacing alloys with the composition of hypoeutectic, eutectic, and hypereutectic at Cr/C6," Tribol. Lett. Vol. 44, pp. 237–245, 2011. https://doi.org/10.1007/s11249-011-9842-2.

[6] K. Wieczerzak, P. Bała, M. Stępień, G. Cios and T. Kozieł, "The characterization of cast Fe-Cr-C alloy," Arch. Metall. Mater., vol. 60, pp. 779–782, 2015. https://doi.org/10.1515/amm-2015-0206.

[7] A. Wiengmoon, J.T.H. Pearce and T. Chairuangsr, "Relationship between microstructure, hardness and corrosion resistance in 20 wt.% Cr, 27 wt.% Cr and 36 wt.% Cr high chromium cast irons," Mater. Chem. Phys., vol.125, pp. 739–748, 2011. https://doi.org/10.1016/j.matchemphys.2010.09.064

[8] J. L. Henderson and J. H. Bulloch, "Alloy classification of hardfacing materials," Int. J. Pres. Ves. Pip., vol. 47, no.2, pp. 127–158, 1991. https://doi.org/10.1016/0308-0161(91)90096-K.

[9] M. Ban, N. Hasegawa, Y. Ueno, H. Shinozaki, T. Aoki and H. Fukumoto, "Wear resistance property of hardfacing weld overlays containing metal carbides," Tribol. Online, vol. 7, no. 4, pp. 207–212, 2012. https://doi.org/10.2474/trol.7.207.

[10] J. M. S. Sa de Sousa, M. Q. Lobato, D. N Garcia and P. C. Machado, "Abrasion resistance of Fe–Cr–C coating deposited by FCAW welding process," Wear, vol. 476, pp. 203688, 2021. https://doi.org/10.1016/j.wear.2021.203688.

[11] Structural Steel - S235, S275, S355 Chemical Composition, Mechanical Properties and Common Applications: https://www.azom.com/article.aspx?ArticleID=6022 [accessed 18/03/2024].

[12] Hardface HC-O https://www.welding-alloys.com/product/hardface-hc-o/ [accessed 18/03/2024].

[13] V. G. Rivlin, "Assessment of phase equilibria in ternary alloys of iron," J. Less-Common Met., vol. 114 no. 1, pp. 111–121, 1985. https://doi.org/10.1016/0022-5088(85)90395-9.

[14] A. V. Khvan, B. Hallstedt and C. Broeckmann. "A thermodynamic evaluation of the Fe–Cr–C system," Calphad, vol. 46, pp. 24–33, 2014. https://doi.org/10.1016/j.calphad.2014.01.002.

[15] C. M. Chang, Y. C. Chen and W. Wu, "Microstructural and abrasive characteristics of high carbon Fe–Cr–C hardfacing alloy," Tribol. Int., vol. 43 no. 5–6, pp. 929–934, 2010. https://doi.org/10.1016/j.triboint.2009.12.045.

[16] A. Inoue and T. Masumoto, "Carbide reactions (M3C→ M7C3→ M23C6→ M6C) during tempering of rapidly solidified high carbon Cr-W and Cr-Mo steels,"Metall. Trans. A, vol. 11, pp. 739–747, 1980.

[17] K. Wieczerzak, P. Bala, R. Dziurka, T.Tokarski, G. Cios, T. Koziel and L. Gondek, "The effect of temperature on the evolution of eutectic carbides and M7C3→ M23C6 carbides reaction in the rapidly solidified Fe-Cr-C alloy," J. Alloys Compd., vol. 698, pp. 673–684, 2017. https://doi.org/10.1016/j.jallcom.2016.12.252.

[18] T. Fras, I. Szachogluchowicz and L. Sniezek, "Ti6Al4V-AA1050-AA2519 explosively-cladded plates under impact loading," Eur. Phys. J. Spec. Top., vol. 227, pp. 17–27, 2018. https://doi.org/10.1140/epjst/e2018-00114-9.

[19] I. Szachogluchowicz, L. Sniezek, T. Slezak, J. Kluczyński, K. Grzelak, J. Torzewski and T. Fras, "Mechanical properties analysis of the AA2519-AA1050-Ti6Al4V explosive welded laminate," Materials, vol. 13, no. 19, pp. 4348, 2020. https://doi.org/10.3390/ma13194348.

[20] C. M. Chang, C. M. Lin, C. C. Hsieh, J.H. Chen and W.Wu, "Microstructural characteristics of Fe–40 wt%Cr–xC hardfacing alloys with [1.0–4.0 wt%] carbon content," J. Alloys Compd., vol. 487, no. 1–2, pp. 83–89, 2009. https://doi.org/10.1016/j.jallcom.2009.07.134.

[21] S. Buytoz, "Microstructural properties of M7C3 eutectic carbides in a Fe-Cr-C alloy," Mater. Lett., vol. 60, pp. 605–608, 2006. https://doi.org/10.1016/j.matlet.2005.09.046.

[22] Y. Matsubara, N. Sasaguri, K. Shimizu and K. Yu, "Solidification and abrasion wear of white cast irons alloyed with 20% carbide forming elements," Wear, vol. 250, pp. 502–510, 2001. https://doi.org/10.1016/S0043-1648(01)00599-3.

[23] A. Bedolla-Jacuinde, B. Hernandez and L. Bejar-Gomez, "SEM study on the M7C3 carbide nucleation during eutectic solidification of high-chromium white irons," Zeitschrift Fuer Met. Res. Adv. Tech. vol. 96, pp. 1380–1385, 2005. https://doi.org/10.3139/146.101188.

[24] Pęcherski RB, Nalepka K, Fras T, Nowak M. Inelastic Flow and Failure of Metallic Solids. Material Effort: Study across Scales. In Constitutive Relations under Impact Loadings (pp. 245-285) Springer Vienna 2014. https://doi.org/10.1007/978-3-7091-1768-2_6

[25] J. T. H. Pearce, "The use of transmission electron microscopy to study the effects of abrasive wear on the matrix structure of a high chromium cast iron," Wear, vol. 89, no. 3, pp. 333–344, 1983. https://doi.org/10.1016/0043-1648(83)90154-0.

[26] S. Ma, J. Xing, Y. He, Y. Li, Z. Huang, G. Liu and Q. Geng, "Microstructure and crystallography of M7C3 carbide in chromium cast iron," Mater. Chem. Phys., vol. 161, pp. 65–73, 2015. https://doi.org/10.1016/j.matchemphys.2015.05.008.

[27] E. Eshed, D. Choudhuri and S. Osovski, "M7C3: The story of a misunderstood carbide," Acta Mater., vol. 235, pp. 117985, 2022. https://doi.org/10.1016/j.actamat.2022.117985.

[28] Jarząbek, D. M., Dziekoński, C., Dera, W., Chrzanowska, J., & Wojciechowski, T. (2018). Influence of Cu coating of SiC particles on mechanical properties of Ni/SiC co-electrodeposited composites. Ceramics International, 44(17), 21750-21758. https://doi.org/10.1016/j.ceramint.2018.08.271

[29] Monnet, A., Guitton, A., Fras, T., Bahi, S., & Rusinek, A. Properties study of a high chromium hardfacing alloy applied to ballistic protection. Post-processing of 20th International Conference On Textures Of Materials ICOTOM 2024. https://sciencesconf.org:icotom20:5223